Eur. Phys. J. A **31**, 810–815 (2007)
DOI 10.1140/epja/i2006-10266-6

THE EUROPEAN PHYSICAL JOURNAL A

Special Article – QNP 2006

Neutron stars as cosmic laboratories to explore hadronic matter at ultra-high densities

I. Bombaci[a]

Dipartimento di Fisica "E. Fermi", Università di Pisa, and INFN, Sezione di Pisa, largo B. Pontecorvo 3, 56127 Pisa, Italy

Received: 23 November 2006
Published online: 19 March 2007 –

Abstract. We examine the present status of the theoretical calculations for the internal structure of neutron stars, and the connection with the microscopic properties of ultradense hadronic matter. We discuss the possibility to have quark deconfinement phase transition in the core of neutron stars, and we explore some of its astrophysical implications as the quark-deconfinement nova model for gamma-ray bursts.

PACS. 97.60.Jd Neutron stars – 26.60.+c Nuclear matter aspects of neutron stars – 24.10.Cn Many-body theory – 25.75.Nq Quark deconfinement, quark-gluon plasma production, and phase transitions

1 Introduction

Neutron stars (NS) are the final product of the evolution of massive stars ($M > 8M_{\odot}$, being $M_{\odot} \simeq 2 \times 10^{33}$ g the mass of the Sun). These stars at the end of their *lives* experience a catastrophic gravitational collapse of their core, which triggers a type-II supernova (SN) explosion and leaves behind a hot and lepton-rich compact remnant (protoneutron star), which within a few minutes evolves to a cold catalyzed configuration (neutron star)[1].

The bulk properties and the internal constitition of NS primarily depend upon the equation of state (EOS) of dense hadronic matter, which is the main ingredient in solving the stellar-structure equations in general relativity [4–6]. Different models for the EOS of dense matter predict a neutron star maximum mass (M_{max}) in the range of 1.4–2.4 $M_{\odot}$, and a corresponding central density n_c in range of 4–10 times the saturation density ($n_0 = 0.16\,\mathrm{fm}^{-3}$) of nuclear matter. In the case of a star with $M \sim 1.4\ M_{\odot}$, different EOS models predict a radius in the range of 7–16 km. Neutron stars are thus the densest macroscopic objects in the Universe. They represent the limit beyond which gravity overwhelm all the other forces of nature and lead to the formation of a black hole.

Due to the large value of the stellar central densities, various regimes (particle species and phases) of dense hadronic matter are expected in the interiors of NS. Consequently, different types of "neutron stars" are hypothesized, as schematically summarized in fig. 1.

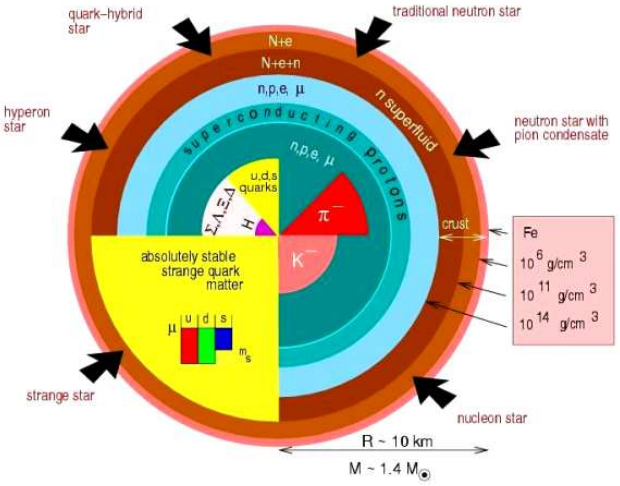

Fig. 1. Schematic cross-section of a neutron star [6].

In the simplest and conservative picture the core of a neutron star is modeled as a uniform fluid of neutron-rich nuclear matter in equilibrium with respect to the weak interaction: these are the so-called "traditional" neutron stars. However, due to the large value of the stellar central density and to the rapid increase of the nucleon chemical potentials with density, hyperons (Λ, Σ^-, Σ^0, Σ^+, Ξ^- and Ξ^0 particles) are expected to appear in the inner core of the star. Other *exotic* phases of hadronic matter such as a Bose-Einstein condensate of negative pion (π^-) or negative kaon (K^-) could be present in the inner part of the star. The core of the more massive NS is also one of the best candidates in the Universe where a phase transition

[a] e-mail: bombaci@df.unipi.it

[1] Under some circumstances the protoneutron star could collapse to a black hole [1–3].

from hadronic matter to a deconfined quark phase could occur. Compact stars which possess a "quark matter core" either as a mixed phase of deconfined quarks and hadrons or as a pure quark matter (QM) phase are called *Hybrid Stars* (HyS) [5]. In the following, the more *conventional* neutron stars in which no fraction of QM is present, will be referred to as *pure Hadronic Stars* (HS).

Even more challenging than the existence of a quark core in a neutron star, is the possible existence of a new type of compact stars consisting completely of a deconfined charge neutral mixture of *up*, *down*, *strange* quarks and electrons, satisfying the hypothesis on the absolute stability [7] of strange-quark matter (SQM). Such compact stars have been called *strange stars* (SS). The analysis of different type of observational data has given indirect evidence for the possible existence of SS (see, *e.g.*, ref. [8]). In the following, we will refer to hybrid stars and strange stars collectively as *Quark Stars* (QS).

Recently, there has been a considerable advance in our understanding of the properties of quark matter. In QCD any attractive quark-quark interaction will lead to pairing and color superconductivity, a subject already addressed in the late 1970s and early 1980s which came back a few years ago since the realization that the typical superconducting gaps in QM may be larger ($\Delta \sim 100\,\mathrm{MeV}$) than those predicted in these early works. The phase diagram of QCD has been analyzed in the light of color superconductivity and model calculations suggest that the phase structure is very rich at high densities (see, *e.g.*, [9,10] and references therein quoted).

Since 1967, the year in which the first radio pulsar was discovered and it was interpreted as a rotating neutron star, the masses of many NS have been measured. The calculated maximum mass, for a given EOS, must be larger than the values of all the measured neutron star masses. Thus, an accurate determination of the mass of NS give a stringent constraint to the global properties of dense matter EOS, and if coupled to additional observable (*i.e.* stellar-radius determination) could allow to discriminate between different possibilities for the internal stellar constitution (presence of hyperons, quark matter, etc.).

Binary stellar systems in which at least one component is a neutron star represent the most reliable way to measure the mass of the compact star. One of the most accurate mass determination is that of the neutron star associated to the pulsar PSR 1913 +16, which is a member of a tight (orbital period equal to 7 h 45 min) neutron star - neutron star system. The mass of PSR 1913 +16 is $1.4408 \pm 0.0003 M_\odot$. Such impressive accuracy is made possible by measuring general relativistic effects, such as the orbital decay due to gravitational radiation, the advance of periastron, the Shapiro delay, etc. Neutron star masses in NS-NS binary systems lie in the range 1.18 to 1.44 $M_\odot$ [11]. However, in at least two accreting X-ray binaries it has been found evidence for compact stars with higher masses. The first of these star is Vela X-1, with a reported mass $1.88 \pm 0.13 M_\odot$ [12], the second is Cygnus X-2, with a reported mass [13] of $1.78 \pm 0.23 M_\odot$. Unfortunately, mass determinations in X-ray binaries are affected by large uncertainties [14], therefore the previous quoted "high mass values" should always be handled with care.

Table 1. Properties of the maximum-mass configuration obtained for different EOS models.

EOS	$M/M_\odot$	R (km)	n_c/n_0
BBB1	1.80	9.70	8.37
BBB2	1.94	9.54	8.31
WFF	2.13	9.40	7.81
APR	2.20	10.10	7.13
BPAL32	1.95	10.54	7.58
KS	2.24	10.79	6.30

Recently Nice *et al.* [15] have determined the mass of the neutron star associated to the millisecond pulsar PSR J0751 +1808, which is a member of a binary system with a helium white dwarf secondary. Measuring general relativistic effects, the authors of ref. [15] have obtained for the mass of PSR J0751 +1808 the value $2.1 \pm 0.2 M_\odot$ at 68% confidence level ($2.1^{+0.4}_{-0.5} M_\odot$ at 95% confidence level). This is the largest measured value for the mass of any neutron star.

2 Traditonal neutron stars

As we said before, in "traditional" neutron stars one assumes the stellar core to be made of an uncharged mixture of neutrons, protons, electrons and muons in equilibrium with respect to the weak interactions (β-stable nuclear matter). Even in this simplified picture, the determination of the EOS remains a formidable theoretical problem. In fact, one has to extrapolate the EOS to extreme conditions of high density and high neutron-proton asymmetry, *i.e.* in a regime where the EOS is poorly constrained by nuclear data and experiments. In the last decade there has been a substantial progress in the microscopic numerical methods for solving the nuclear many-body problem both within the non-relativistic and relativistic approaches. For example, the convergence of the Brueckner-Bethe-Goldstone (BBG) hole line expansion has beed inspected up to the three-hole line contribution [16] in the continuous choice for the auxiliary single-particle potential. The introduction of nuclear three-body forces (TBF) constrained by nuclear data [17] has permitted to solve the *saturation problem* of nuclear matter in the non-relativistic approach [18–20].

In table 1, we report the maximum-mass configuration of NS using different EOS. The first two stellar models (BBB) have been obtained [19] within the Brueckner-Hartree-Fock (BHF) approximation of the BBG theory. Model BBB1 makes use of the Argonne v14 (Av14) nucleon-nucleon (NN) interaction implemented by the Urbana TBF. Model BBB2, considers the Paris NN interaction and the Urbana TBF. We next consider two stellar models (WFF, APR) which are based on microscopic EOSs derived by variational chain summation methods. The WFF model [18] makes use of the Av14 interaction plus the Urbana (model VII) TBF. The APR model [20] is

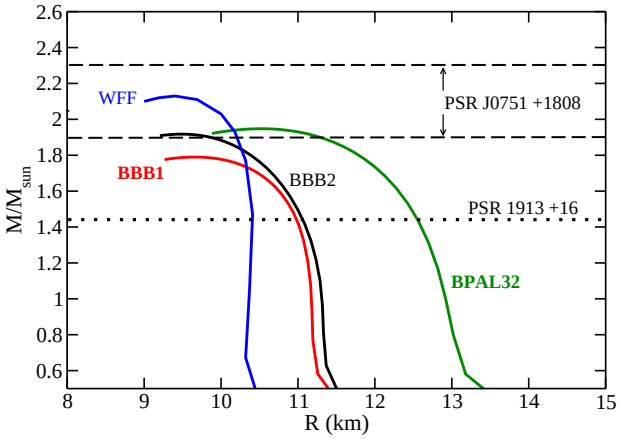

Fig. 2. The mass-radius relation for neutron stars for different EOS for β-stable nuclear matter. The dotted line gives the value of the mass of PSR 1913 +16, the band between the long-dashed lines the mass of PSR J0751 +1808 (at 68% c.l.).

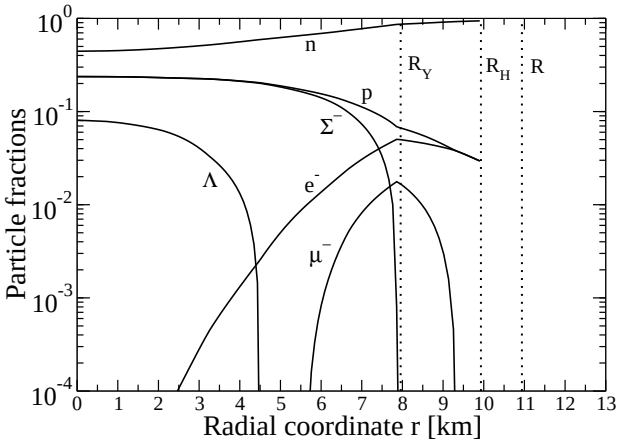

Fig. 3. The internal composition of a neutron star with hyperonic-matter core. R_Y is the radius of the hyperonic core. The nuclear-matter layer extend between R_Y and R_H. The stellar crust extend between R_H and R.

based on the charge-dependent Argonne v18 (Av18) two-body potential plus the Urbana (model IX) TBF. In addition, the APR model includes boost corrections to the NN interaction, which give the leading relativistic corrections to the EOS. The BPAL 32 neutron star configurations have been calculated using a phenomenological EOS for asymmetric nuclear matter [21] (see also [3,22]) derived from a momentum- and density-dependent effective NN interaction. The BPAL model is an extension of the EOS of refs. [23,24]. An important feature of the BPAL EOS is the possibility to have different forms for the density dependence of the potential part of the nuclear symmetry energy, reproducing different results predicted by various microscopic calculations. The nuclear symmetry energy E_{sym} (particularly its density dependence) plays an important role in the physics of NS. In fact, $E_{sym}(n)$ affects the values of the stellar radius [22,25], the values of the threshold densities for the onset of various new particle species (*e.g.*, K^- condensation [26], hyperons, QM phase [27]) and the value of the proton fraction in the stellar core [24,19]. The latter quantity has a strong influence on the thermal evolution of neutron stars. Finally, we consider a stellar model (KS) based on a miscroscopic EOS derived [28] from the Dirac-BHF approach using the Bonn-B nuclear interaction. The mass radius relations for some of these stellar models are reported in fig. 2, together with the measured values of the masses of PRS 1913 +16 and PSR J0751 +1808.

3 Hyperon stars

The reason why hyperons are expected in the high dense core of a neutron star is very simple, and it is mainly a consequence of the fermionic nature of nucleons, which makes the nucleon chemical potentials a very rapidly increasing function of density. As soon as the chemical potential of neutrons becomes sufficiently large, the most energetic neutrons (*i.e.*, those on the Fermi surface) can decay via the weak interactions into Λ hyperons and form a Fermi sea of this new hadronic species with $\mu_\Lambda = \mu_n$. The Σ^- can be produced via the process $e^- + n \to \Sigma^- + \nu_e$ when the Σ^- chemical potential fulfill the condition[2] $\mu_{\Sigma^-} = \mu_n + \mu_e$. Hyperons appear at a relatively moderate density of about 2 times n_0. Notice that the Σ^- hyperon appears at a lower density than the Λ, even though the Σ^- is more massive than the Λ. This is due to the contribution of the electron chemical potential μ_e to the threshold condition for the Σ^- (*i.e.*, $M_{\Sigma^-} = \mu_n + \mu_e$, for free hyperons) and to the fact that μ_e in dense matter is large and can compensate for the mass difference $M_{\Sigma^-} - M_\Lambda = 81.76\,\mathrm{MeV}$.

In fig. 3, we show the radial profile of a typical hyperon star [29]. As we see the hyperonic-matter inner core of the star extend for about 8 km. This radius has to be compared with the total stellar radius $R \sim 11\,\mathrm{km}$, and with the thickness of the nuclear-matter layer (outer core) which is about 2 km.

The influence of hyperons on neutron stars properties has been investigated using different approaches to determine the EOS of hyperonic matter. One of the most popular approaches, to solve this problem, is the relativistic mean-field model [30,5]. Some of the parametrizations of the Lagrangian of the theory have tried to reconcile measured values of neutron star masses with the binding energy of the Λ particle in hypernuclei [31]. Considerable progress has been done in the last few years in microscopic calculations of hyperonic matter. This method is based on an extension of the BBG theory to include hyperonic degrees of freedom [32,33,29]. In particular, the study of ref. [29] focus on the properties of a newborn neutron star, and explore the consequences of neutrino trapping in dense matter on the structural properties and on the early evolution of neutron stars [3].

[2] Except from the very initial stage soon after neutron star birth, neutrinos freely escape the star and thus the neutrino chemical potentials can be put equal to zero.

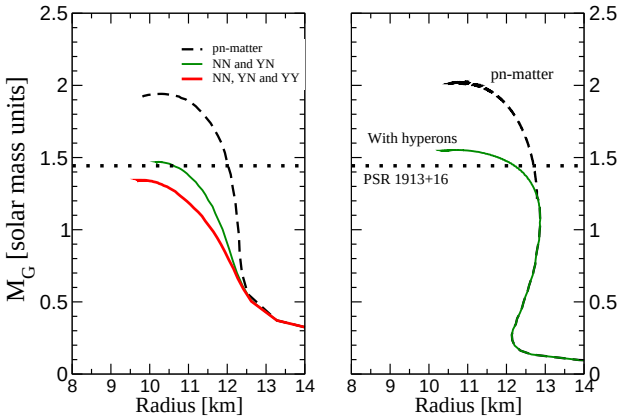

Fig. 4. Mass-radius relation for "traditional" neutron stars and hyperon stars calculated [33] within the BHF approach with the NSC9e interaction (left panel) and with the relativistic mean-field EOS GM3 of ref. [31] (rigth panel). The dotted horizontal line indicates the mass of PSR1913+16.

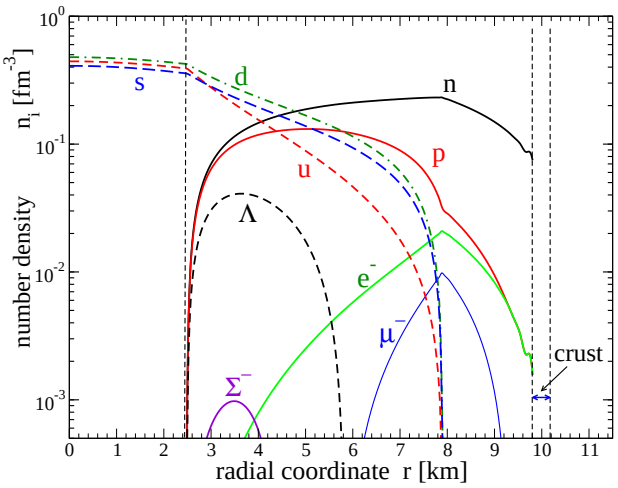

Fig. 5. Internal composition of a hybrid star with $M = M_{max} = 1.448\ M_\odot$. The GM3 EOS [31] has been used for the hadronic phase, and the bag model EOS, with $B = 136.6\,\mathrm{MeV/fm^3}$ and $m_s = 150\,\mathrm{MeV}$, for the quark phase.

As expected, the presence of hyperons reduces in a sizeable manner the value of the pressure of β-stable hyperonic matter with respect to the case of β-stable nuclear matter at the same density. This softening of the EOS has important consequences on many macroscopic properties of the star: the maximum mass is reduced by $\Delta M_{max} \sim 0.5$–$0.8\ M_\odot$, and the corresponding central density is increased. Also, hyperon stars are more compact (*i.e.* they have a smaller radius) with respect to traditional neutron stars. This is illustrated in fig. 4, where we show the mass-radius relation for traditional neutron stars and for hyperon stars obtained with the microscopic EOS of ref. [33] (left panel) and with the relativistic mean-field EOS (GM3 model) given in ref. [31]. The results depicted in fig. 4 clearly demonstrate that to neglect hyperons leads to an overstimate of M_{max}.

It is important to notice the "low" value of the stellar maximum mass, predicted within the approach of ref. [33], which is in contrast with the measured mass of PSR 1913 +16. The prediction of a value for M_{max} below some of the measured neutron star masses is a common feature of all the present microscopic EOS of hyperonic matter based on G-matrix BHF calculations [32,33,29]. For example, the authors of ref. [32], in case of the Argonne v_{18} NN interaction, found $M_{max} = 2.00\ M_\odot$, a corresponding radius of $R = 10.54\,\mathrm{km}$ and a central density $\rho_c = 1.11\,\mathrm{fm^{-3}}$ for neutron stars with a pure nucleonic core. When hyperons are considered as possible stellar constituents, they found [32] $M_{max} = 1.22\ M_\odot$, a corresponding radius of $R = 10.46\,\mathrm{km}$ and a central density $\rho_c = 1.25\,\mathrm{fm^{-3}}$. Therefore the current EOS for hyperonic matter, deduced from microscopic G-matrix BHF calculations, are "too soft" to explain observed neutron star masses.

Clearly, one should try to trace the origin of this problem back to the underlying YN and YY two-body interactions or to the possible repulsive three-body baryonic forces involving one or more hyperons, not included in the work of refs. [32,33,29]. Presently, this is a subject of very active research by people working in this field. Therefore, the use of microscopic EOS of hyperonic matter in the contest of neutron star physics is of fundamental importance for our understanding of the strong interactions involving hyperons, and to learn how these interactions behave in dense many-body systems.

4 Hybrid stars

As we have seen before, different sophisticated approaches, based on advanced many-body thecniques, have been utilized to derive the EOS for the hadronic phase. This is possible, to a large extent, thanks to the rich body of experimantal data at density $n \sim n_0$. The situation is drastically different in the case of quark matter. Presently, only indirect experimental evidence has been found for the existence of this new phase of matter. Moreover, lattice QCD calculations at finite density, to derive the EOS of quark matter, are still in an early stage. Thus, simple phenomenological (*e.g.*, MIT bag, Nambu–Jona-Lasinio) models have been used to describe QM for hybrid-star calculations.

In fig. 5, we show the typical internal composition of a hybrid star. The cross-section of the star is relative to the maximum-mass configuration ($M = M_{max} = 1.448 M_\odot$, with radius $R = 10.2\,\mathrm{km}$, and central density $\rho_c = 28.1 \times 10^{14}\,\mathrm{g/cm^3}$) for the EOS described in the figure caption. This star has a pure QM core which extend for about 2.5 km, next it has a hadron-quark mixed phase layer with a thickness of about 5.5 km, followed by a nuclear matter layer about 2 km thick. On the top we have the usual neutron star crust. The presence of quarks makes the EOS softer with respect to the corresponding pure hadronic-matter EOS. The stellar sequence associated to the latter EOS has the maximum-mass configuration: $M_{max} = 1.552\ M_\odot$, $R = 10.7\,\mathrm{km}$, $\rho_c = 25.4 \times 10^{14}\,\mathrm{g/cm^3}$.

Many possible astrophysical signals for the presence of a quark core in neutron stars have been proposed (see [5,6]

and references quoted therein). Particularly, pulse timing properties of pulsars have attracted much attention since they are a manifestation of the rotational properties of the associated neutron star. The onset of quark-deconfinement in the core of the star, will cause a change in the stellar moment of inertia [34]. This change will produce a peculiar evolution of the stellar rotational period ($P = 2\pi/\Omega$) which will cause large deviations of the so-called pulsar braking index $n(\Omega) = (\Omega\ddot{\Omega}/\dot{\Omega}^2)$ from the *canonical* value $n = 3$, derived within the magnetic-dipole model for pulsars and assuming a constant moment of inertia for the star. The possible measurement of a value of the braking index very different from the canonical value (*i.e.* $|n| \gg 3$) has been proposed [34] as a signature for the occurrence of the quark-deconfinement phase transition in a neutron star. However, it must be stressed that a large value of the braking index could also results from the pulsar magnetic-field decay or alignment of the magnetic axis with the rotation axis [35].

5 Metastability of hadronic stars and GRBs

In bulk matter the quark-hadron mixed phase begins at the *static transition point* defined according to the Gibbs' criterion for phase equilibrium

$$\mu_H = \mu_Q \equiv \mu_0, \qquad P_H(\mu_0) = P_Q(\mu_0) \equiv P_0, \qquad (1)$$

where $\mu_H = (\varepsilon_H + P_H)/n_{b,H}$ and $\mu_Q = (\varepsilon_Q + P_Q)/n_{b,Q}$ are the chemical potentials for the hadron and quark phase respectively, ε_H (ε_Q), P_H (P_Q) and $n_{b,H}$ ($n_{b,Q}$) denote respectively the total (*i.e.*, including leptonic contributions) energy density, the total pressure and baryon number density for the hadron (quark) phase.

Consider now the more realistic situation in which one takes into account the energy cost due to finite-size effects in creating a drop of QM in the hadronic environment. As a consequence of these effects, the formation of a critical-size drop of QM is not immediate and it is necessary to have an overpressure $\Delta P = P - P_0$ with respect to the static transition point. Thus, above P_0, hadronic matter is in a metastable state, and the formation of a real drop of QM occurs via a quantum nucleation mechanism. Quark flavor must be conserved during the deconfinement transition [36]. We will call this form of deconfined matter, in which the flavor content is equal to that of the β-stable hadronic system at the same pressure, as the Q*-phase. Soon afterwards a critical-size drop of QM is formed the weak interactions will have enough time to act, changing the quark flavor fraction of the deconfined droplet to lower its energy, and a droplet of β-stable SQM is formed (hereafter the Q-phase).

In the scenario proposed in ref. [37], one considers a pure HS whose central pressure is increasing due to spin-down or due to mass accretion, *e.g.*, from the material left by the SN explosion, or from a companion star. As the central pressure exceeds the threshold value P_0^* at the static transition point, a virtual drop of quark matter in the Q*-phase can be formed in the center of the star. As soon as a real drop of Q*-matter is formed, it will grow very rapidly and the original HS will be converted to and hybrid star or to a strange star, depending on the detail of the EOS for quark matter employed to model the phase transition. The nucleation time τ (*i.e.*, the time needed to form the first critical droplet of QM), can be calculated for different values of the stellar central pressure P_c, and thus for different values of the mass $M(P_c)$ of the corresponding hadronic star. The nucleation time τ dramatically depends on [37] the value of the stellar mass (central pressure). A metastable hadronic star can have a mean lifetime many orders of magnitude larger than the age of the Universe. As the star accretes a small amount of mass (of the order of a few per cent of the mass of the Sun), the consequential increase of the central pressure leads to a huge reduction of the nucleation time and, as a result, to a dramatic reduction of the HS *mean lifetime*.

To summarize, pure hadronic stars having a central pressure larger than the static transition pressure P_0^* for the formation of the Q*-phase are metastable to the *decay* (conversion) to a more compact stellar configuration in which deconfined QM is present (HyS or SS). These metastable HS have a *mean lifetime*[3] which is related to the nucleation time to form the first critical-size drop of deconfined matter in their interior. We define as *critical mass* M_{cr} of the metastable HS, the value of the gravitational mass for which the nucleation time is equal to one year: $M_{cr} \equiv M_{HS}(\tau = 1\,\mathrm{y})$. Pure hadronic stars with $M_H > M_{cr}$ are very unlikely to be observed. M_{cr} plays the role of an *effective maximum mass* [36] for the hadronic branch of compact stars. While the Oppenheimer-Volkoff maximum mass [4] $M_{HS,max}$ is determined by the overall stiffness of the EOS for hadronic matter, the value of M_{cr} will depend in addition on the bulk properties of the EOS for quark matter and on the properties at the interface between the confined and deconfined phases of matter (*e.g.*, the droplet surface tension σ).

In fig. 6, we show the mass-radius (MR) curve for pure HSs within the GM1 [31] EOS for the hadronic phase, and that for hybrid or strange stars for different values of the bag constant B. The configuration marked with an asterisk on the hadronic MR curves represents the HS for which the central pressure is equal to P_0^* and $\tau = \infty$. The full circle on the HS sequence represents the critical-mass configuration, in the case of $\sigma = 30\,\mathrm{MeV/fm^2}$. The full circle on the HyS (SS) mass-radius curve represents the hybrid (strange) star which is formed from the conversion of the hadronic star with $M_{HS} = M_{cr}$. We assume that during the stellar-conversion process the total number of baryons in the star (*i.e.*, the stellar baryonic mass) is conserved. Thus, the total energy liberated in the stellar conversion is given [38] by the difference between the gravitational mass of the initial hadronic star ($M_{in} \equiv M_{cr}$) and that of the final hybrid or strange stellar configuration $M_{fin} \equiv M_{QS}(M_{cr}^b)$ with the same baryonic mass: $E_{conv} = (M_{in} - M_{fin})c^2$.

[3] The actual *mean lifetime* of the HS depends on the mass accretion or on the spin-down rate which modifies τ via an explicit time dependence of the stellar central pressure.

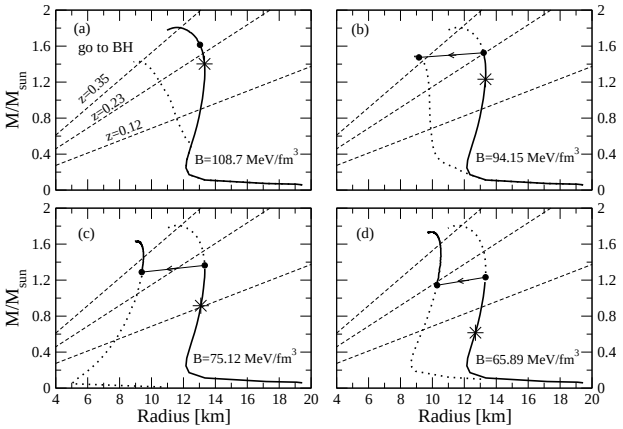

Fig. 6. Mass-radius relation for pure HSs [36] and for HyS or SS configurations for several values of the bag constant. The configuration marked with an asterisk represents the HS for which the central pressure is equal to P_0^* and $\tau = \infty$. The conversion process of the HS, with a mass equal to M_{cr}, into a final QS is denoted by the full circles connected by an arrow. In all cases $\sigma = 30\,\mathrm{MeV/fm^2}$. The dashed lines show the gravitational red shift deduced for the X-ray compact sources EXO 0748-676 ($z = 0.35$) and 1E 1207.4-5209 ($z = 0.12$–0.23).

The stellar-conversion process, described so far, will start to populate the new branch of quark stars (the part of the QS sequence plotted as a continuous curve in fig. 6). Long-term accretion on the QS can next produce stars with masses up to the limiting mass $M_{QS,max}$ for the quark star configurations.

The stellar conversion energy E_{conv} is in the range [36] 0.5–1.7×10^{53} erg. This mechanism has been proposed as a possible energy source for Gamma Ray Bursts (GRBs). The model of ref. [37] accounts for the association between SN explosions and GRBs, in fact, the stellar conversion represents a second "explosion" (the *Quark Deconfinement Nova* [36]) which occurs after the first explosion (the SN) which form the hadronic star. This model is also able to explain, in a natural way, the possibility to have a *long*-time delay ΔT between the SN explosion and the associated GRB, as inferred, for example, in the case of GRB990705 ($\Delta T \sim$ a few years) [39], GRB011211 ($\Delta T \sim$ a few days) [40].

References

1. G.E. Brown, H.A. Bethe, Astrophys. J. **423**, 659 (1994).
2. I. Bombaci, Astron. Astrophys. **305**, 871 (1996).
3. M. Prakash, I. Bombaci, M. Prakash, P.J. Ellis, R. Knorren, J.M. Lattimer, Phys. Rep. **280**, 1 (1997).
4. J.R. Oppenheimer, G.M. Volkoff, Phys. Rev. **62**, 035801 (2000).
5. N.K. Glendenning, *Compact Stars: Nuclear Physics, Particle Physics, and General Relativity* (Springer Verlag, 1996).
6. F. Weber, *Pulsars as Astrophysical Laboratories for Nuclear and Particle Physics* (IoP Publishing, 1999).
7. A.R. Bodmer, Phys. Rev. D **4**, 1601 (1971); H. Terazawa, INS Report **336** (Tokio University, 1979); E. Witten, Phys. Rev. D **30**, 272 (1984).
8. X.-D Li, I. Bombaci, M. Dey, J. Dey, E.P.J. van den Heuvel, Phys. Rev. Lett. **83**, 3776 (1999).
9. M.G. Alford, Annu. Rev. Nucl. Part. Sci. **51**, 131 (2001).
10. G. Nardulli, Riv. Nuovo Cimento **25**, 1 (2001).
11. S.E. Thorsett, D. Chakrabarty, Astrophys. J. **512**, 288 (1999).
12. H. Quaintrell *et al.*, Astron. Astrophys. **401**, 313 (2003).
13. J.A. Orosz, E. Kuulkers, Mon. Not. R. Astron. Soc. **305**, 1 (1999).
14. M.H. van Kerkwijk *et al.*, Astron. Astrophys. **303**, 483 (1995).
15. D.J. Nice *et al.*, Astrophys. J. **634**, 1242 (2005).
16. H.Q. Song *et al.*, Phys. Rev. Lett. **81**, 1584 (1998).
17. B.S. Pudliner *et al.*, Phys. Rev. Lett. **74**, 4396 (1995).
18. R.B. Wiringa, V. Ficks, A. Fabrocini, Phys. Rev. C **38**, 1010 (1988).
19. M. Baldo, I. Bombaci, G.F. Bugio, Astron. Astrophys. **328**, 274 (1997).
20. A. Akmal, V.R. Pandharipande, D.G. Ravenhall, Phys. Rev. C **58**, 1804 (1998).
21. I. Bombaci, in *Perspectives on Theoretical Nuclear Physics, Proceedings of the Conference Problems in Theoretical Nuclear Physics, October 1995, Cortona (Italy)*, edited by I. Bombaci *et al.* (ETS, Pisa, 1996) p. 223.
22. I. Bombaci, in *Isospin Physics in Heavy-Ion Collisions at Intermediate Energies*, edited by B.-A. Li, W.U. Schröder (Nova Science Publisher, New York, 2001) p. 35.
23. C. Gale, G, Bertsch, S. Das Gupta, Phys. Rev. C **35**, 1666 (1997).
24. M. Prakash, T.L. Ainsworth, J.M. Lattimer, Phys. Rev. Lett. **61**, 2518 (1998).
25. B.-A. Li, A.W. Steiner, Phys. Lett. B **642**, 436 (2006).
26. W. Zuo *et al.*, Phys. Rev. C **70**, 055802 (2004).
27. M. Di Toro *et al.*, Nucl. Phys. A **775**, 102 (2006).
28. P.G. Krastev, F. Sammarruca, Phys. Rev. C **74**, 025808 (2006).
29. I. Vidaña, I. Bombaci, A. Polls, A. Ramos, Astron. Astrophys. **399**, 687 (2003).
30. N.K. Glendenning, Astrophys. J. **293**, 470 (1985).
31. N.K. Glendenning, S.A. Moszkowski, Phys. Rev. Lett. **67**, 2414 (1991).
32. M. Baldo, G.F. Burgio, H.J. Schulze, Phys. Rev. C **61**, 055801 (2000).
33. I. Vidaña, A. Polls, A. Ramos, L. Engvik, M. Hjorth-Jensen, Phys. Rev. C **62**, 035801 (2000).
34. N.K. Glendenning, S. Pei, F. Weber, Phys. Rev. Lett. **79**, 1603 (1997).
35. T.M. Tauris, S. Konar, Astron. Astrophys. **376**, 543 (2001).
36. I. Bombaci, I. Parenti, I. Vidaña, Astrophys. J. **614**, 314 (2004).
37. Z. Berezhiani, I. Bombaci, A. Drago, F. Frontera, A. Lavagno, Astrophys. J. **586**, 1250 (2003).
38. I. Bombaci, B. Datta, Astrophys. J. **530**, L72 (2000).
39. L. Amati *et al.*, Science **290**, 953 (2000).
40. J.N. Reeves *et al.*, Nature **414**, 512 (2002).